The Journal of Experimental Biology 213, 3920-3933
© 2010. Published by The Company of Biologists Ltd
doi:10.1242/jeb.046706

The mechanics of the adhesive locomotion of terrestrial gastropods

Janice H. Lai[1,2,*], Juan C. del Alamo[1], Javier Rodríguez-Rodríguez[1,3] and Juan C. Lasheras[1,4]

[1]Department of Mechanical and Aerospace Engineering, University of California, San Diego, La Jolla, CA 92093-0411, USA, [2]Department of Mechanical Engineering, Stanford University, Building 530, 440 Escondido Mall, Stanford, CA 94305-3030, USA,[3]Departamento de Ingeniería Térmica y de Fluidos, Universidad Carlos III de Madrid, 28911 Leganés, Spain and [4]Department of Bioengineering, University of California, San Diego, La Jolla, CA 92093, USA

*Author for correspondence (jhlai@stanford.edu)

Accepted 23 August 2010

SUMMARY

Research on the adhesive locomotion of terrestrial gastropods is gaining renewed interest as it provides a source of guidance for the design of soft biomimetic robots that can perform functions currently not achievable by conventional rigid vehicles. The locomotion of terrestrial gastropods is driven by a train of periodic muscle contractions (pedal waves) and relaxations (interwaves) that propagate from their tails to their heads. These ventral waves interact with a thin layer of mucus secreted by the animal that transmits propulsive forces to the ground. The exact mechanism by which these propulsive forces are generated is still a matter of controversy. Specifically, the exact role played by the complex rheological and adhesive properties of the mucus is not clear. To provide quantitative data that could shed light on this question, we use a newly developed technique to measure, with high temporal and spatial resolution, the propulsive forces that terrestrial gastropods generate while crawling on smooth flat surfaces. The traction force measurements demonstrate the importance of the finite yield stress of the mucus in generating thrust and are consistent with the surface of the ventral foot being lifted with the passage of each pedal wave. We also show that a forward propulsive force is generated beneath each stationary interwave and that this net forward component is balanced by the resistance caused by the outer rim of the ventral foot, which slides at the speed of the center of mass of the animal. Simultaneously, the animal pulls the rim laterally inward. Analysis of the traction forces reveals that the kinematics of the pedal waves is far more complex than previously thought, showing significant spatial variation (acceleration/deceleration) as the waves move from the tail to the head of the animal.

Supplementary material available online at http://jeb.biologists.org/cgi/content/full/213/22/3920/DC1

Key words: propulsive force, adhesive locomotion, invertebrate.

INTRODUCTION

Despite the lack of extremities, terrestrial gastropods are able to crawl steadily using their belly (or ventral foot) as the single locomotory organ. Understanding this locomotion mechanism has been a subject of interest to biologists and biophysicists for over a century. The prospect of novel robotic designs that mimic this adhesive locomotion (Chan et al., 2007; Kim et al., 2006) has renewed interest in the subject among engineers and physicists. Although physical observations and physiological knowledge exist regarding terrestrial gastropod locomotion, the mechanics of pedal waves and their contribution to the generation of the propulsive forces remain unclear.

It is well established that, during gastropod locomotion, a series of pulses of muscle contraction and relaxation travel along the central portion of the foot's ventral surface (Fig. 1). These pulses of muscular activity, whose propagation speed, V_{wave}, is greater than the speed of the animal, are known as pedal waves. The regions of the foot between consecutive pedal waves, where the foot remains stationary with respect to the ground, are called interwaves. The distance between the center of two consecutive pedal waves is called the wavelength, and it is usually much greater than the length of the pedal waves themselves. Therefore, a large portion of the animal's ventral foot is occupied by the interwaves and does not move during locomotion. The central portion of the foot, where the pedal waves responsible for active crawling are located, is surrounded by the rim, which moves at the speed of the body (centroid) of the animal (Fig. 1).

Dubois and Vles classified the waves observed in the rhythmic locomotion of gastropods according to their number and propagating direction (Dubois and Vles, 1907). The foot of the terrestrial gastropod may contain a single train of pedal waves (monotaxic) or be divided structurally into two (ditaxic) or four (tetrataxic) series of waves. These waves may move from the posterior to the anterior part of the animal (direct waves) or the reverse (retrograde waves). However, all gastropods, irrespective of the direction of propagation of the pedal waves (direct or retrograde), are restricted to forward locomotion and, unlike earthworms, cannot reverse the direction of propagation of the waves to move backwards (Parker, 1911). Most terrestrial gastropods such as slugs and snails propel themselves through direct monotaxic waves. Retrograde waves are found mainly in marine gastropods. It is generally agreed that direct pedal waves are longitudinally contracted whereas retrograde waves are longitudinally extended (Crozier and Pilz, 1924; Denny, 1981; Jones, 1973; Lissmann, 1945a; Lissmann, 1945b). Crozier and Pilz measured the speed and frequency of the pedal waves and concluded that these waves are spaced evenly (constant wavelength) and that their number is invariant for each animal, although it might increase during rapid crawling (Crozier and Pilz, 1924). They found that the crawling speed of gastropods is directly proportional to the speed of the pedal waves and to the frequency at which they are generated. However, our observations reported here show that neither the wavelength nor the speed of individual waves remains constant, raising the question of the possible significance of this variation.

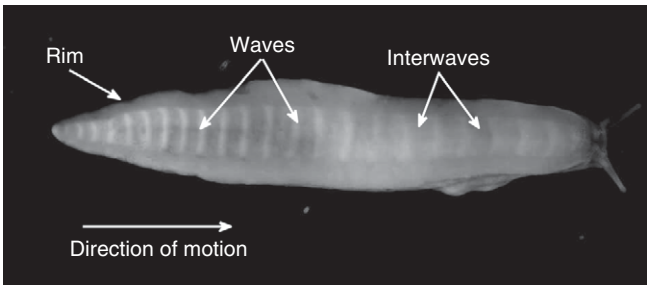

Fig. 1. The ventral surface of a banana slug (*Ariolimax californicus*) moving over a glass surface from left to right. A single train of 23 waves (white bands) and interwaves as well as the rim of the ventral surface can be clearly visualized. Observe that the distance between waves (wavelength) is not constant as the waves move from tail to head.

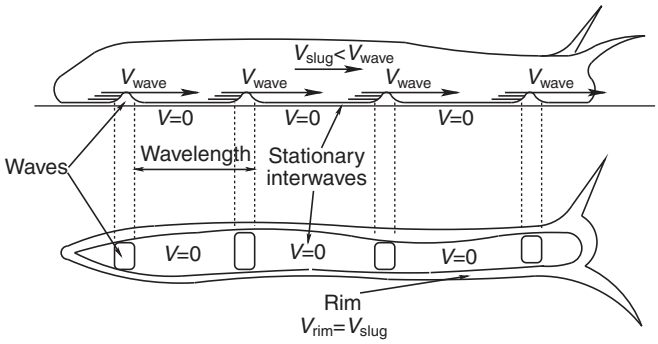

Fig. 2. Sketch of the side view (top) and the ventral foot (bottom) of a terrestrial gastropod showing the location of the waves, interwaves and rim. The animal is moving from left to right. The vertical displacements associated with the pedal waves are not to scale. V_{wave}, speed of the pedal waves; V, speed of the interwaves; V_{slug}, overall crawling speed of the animal; V_{rim}, speed of the rim.

Lissmann established a general picture of the mechanics of the pedal waves and their contribution to the overall movement of gastropods (Lissmann, 1945a; Lissmann, 1945b). He made accurate measurements of the progression of different regions of a snail's foot during locomotion, showing that the interwave regions remain stationary whereas the regions of the foot within the waves travel along the ventral foot at a speed considerably faster than the forward velocity of the body (center of mass). He also measured the shear forces exerted at a fixed location of the substrate as the animal passed over it and showed that a forward propulsive force is generated in the mid-section of the foot whereas sliding friction appears at the anterior and posterior ends of the animal.

The geometry of pedal waves has long been a subject of controversy. Several early studies stated that pedal waves are concavities on the foot, as depicted in Fig. 2 (Crozier and Pilz, 1924; Jones, 1973; Parker, 1911). Parker reported that the waves are slight concavities as evidenced by the distortion of air bubbles embedded in the mucus underneath the foot (Parker, 1911). As a wave approaches the air bubble, the bubble is squeezed laterally and moves towards the center of the wave, suggesting a slight suction effect caused by the wave. As the wave leaves the air bubble, the bubble is elongated longitudinally, implying that it is being pressed against the substrate. Jones further confirmed the concavity of the pedal waves with direct observation of slug (*Agriolimax reticulatus*) feet that had been frozen during crawling (Jones, 1973). However, Denny did not observe concavities in frozen samples of the foot of Pacific banana slugs (*Ariolimax columbianus*) and, based on estimations of the force required to fill the lifted wave space with pedal mucus, concluded that the pedal waves must always remain attached to the substrate when the animal crawls on a flat, smooth surface (Denny, 1981).

The pedal waves, along with the adhesive properties of the mucus layer, create the stable thrust needed for the animal to crawl on substrates at various inclinations. In most terrestrial gastropods, such as common garden snails and slugs, two types of mucus are generated during locomotion: a thick pedal mucus secreted through the glands located underneath the animal's mouth and a much thinner mucus secreted through multiple glands located on the sole of the animal (Barr, 1926; Barr, 1927). It is clear that the mucus plays a key role in the ability of gastropods to lubricate their sliding motion while adhering firmly to the substrate at various inclinations. Denny and Gosline performed a series of very interesting measurements of gastropod locomotion with an emphasis on the role that the rheology of the pedal mucus plays in the generation of pedal forces (Denny, 1981; Denny and Gosline, 1980). In particular, Denny studied the mechanics of the thin layer of mucus that lies between the substrate and the foot and categorized the movement as 'adhesive locomotion' (Denny, 1981). He measured the rheological properties of the pedal mucus and concluded that the viscoelastic nature of the mucus provides a mechanism for the generation of the net friction needed to propel the animal forward using direct pedal waves. More recently, Lauga and Hosoi constructed a mathematical model of lubrication and adhesive locomotion built upon the hypothesis established by Denny, and demonstrated that the non-Newtonian nature of pedal mucus can result in the generation of a net propulsive force using direct pedal waves (Lauga and Hosoi, 2006).

An important question that still remains open is to what extent the observed rheological properties of the mucus are required to produce thrust. It is widely accepted that mucus is necessary for adhesion and lubrication of the foot, but its role in the precise mechanism of thrust generation is unclear. Notice that whereas, in the case of retrograde crawlers (Chan et al., 2005), a peristaltic mechanism similar to that found in earthworms (Quillin, 1999) would suffice to produce thrust regardless of the rheology of the mucus or whether the foot is lifted, crawlers exhibiting direct waves need to either lift the foot during the passage of the pedal wave or rely on the shear-thinning characteristics of the mucus (Lauga and Hosoi, 2006). Lifting the forward-moving part of the foot to reduce the drag is analogous to the way in which a caterpillar crawls (Brackenbury, 1999) and would require no particular rheological properties of the mucus. However, if it is assumed that the foot remains flat throughout movement, propulsion can only be achieved by taking advantage of the finite yield stress of the mucus as described by Chan et al. (Chan et al., 2005). One cannot discard the possibility that terrestrial gastropods generate their thrust from a combination of these modes, as they need to be able to crawl over a vast variety of surfaces. Deciphering this versatility is highly relevant from the point of view of biomimetic engineering, as it would allow for designs of mechanical robots that are able to adhere to and move in a wide range of conditions.

The principal aim of the present study is to provide detailed experimental measurements that may help clarify the precise propulsion mechanism that takes place in terrestrial gastropods during locomotion. Specifically, we analyzed the kinematics and the dynamics of pedal waves using high-resolution measurements of the propulsive and friction forces exerted on the substrate by moving

gastropods. These measurements were obtained using a newly developed force-cytometry method that consists of calculating the spatial and temporal distribution of pedal forces from measurements of the deformation produced by the animal on substrates of known elastic properties (del Alamo et al., 2008). Our method allows us to study in great detail the propulsion mechanics while simultaneously measuring the most important aspects of the kinematics of the motion, including pedal wave speed, animal crawling speed and pedal wave frequency. One of the key innovations of our experimental procedure is that it allows the measurement of the horizontal traction stresses applied on the substrate's surface underneath the animal, without any optical interference from the animal's body. Other previously described methods (e.g. Full et al., 1995; Harris et al., 1980; Harris, 1978) rely on the characteristics of the light transmitted through the substrate, thus the presence of the animal precludes the measurement of the stress field directly underneath the body and its extremities. Although the above techniques are extremely useful when one is interested in measuring the force exerted by animals with small feet, such as cockroaches, they are very much restricted in the study of gastropods.

Our force measurements revealed that each stationary interwave produced a net thrust force whereas each moving wave generated a lower net resistance force, possibly owing to the lifting of the waves. Therefore, each wave–interwave pair generated a net thrust force that was balanced by the sliding friction caused by the rim, head and tail of the animal. We found that the level of force generated under the interwaves correlated positively with the animal's length. This result is interesting because it explains our observation that faster animals have fewer waves on the ventral surface.

A secondary aim of this study was to analyze the kinematics of the pedal waves (wave speed and frequency) and its significance in the generation of traction force. This aim was motivated by our unexpected observations that the spatiotemporal organization of the pedal waves (wavelength and speed) in all species of terrestrial gastropods that we studied (*Deroceras reticulatum*, *Helix aspersa*, *Ariolimax californicus* and *A. buttoni*) is much more complex than previously reported (Crozier and Pilz, 1924; Denny, 1981; Jones, 1973; Lissmann, 1945a; Lissmann, 1945b). We therefore conducted experiments to answer the following questions about the possible role of the pedal waves in the propulsion: (1) What is the relationship between the speed/wavelength of these waves and the velocity of translocation of the animal? (2) Do these waves maintain a constant speed/wavelength as they propagate along the foot when the animal's center of mass translocates at constant velocity? (3) How does the animal accelerate or decelerate its speed? (4) Is this change in speed achieved by increasing the number of waves or by varying their speed and wavelength?

MATERIALS AND METHODS

We performed two sets of experiments to investigate the kinematics and dynamics of terrestrial gastropod locomotion. The first set of experiments focused on the kinematics and consisted of measuring the relationship between the speed of propagation of the pedal waves and the crawling speed of these animals. The second set of experiments was designed to study the role of the pedal waves in the generation of the traction forces by performing fine-resolution measurements of the spatial and temporal distribution of the stresses exerted by the animal on the substrate during crawling.

The experiments were performed using gray garden slugs [*Deroceras reticulatum* (Müller 1774)] and garden snails [*Helix aspersa* (Müller 1774)]. All were collected in San Diego, CA, USA. In addition, we obtained measurements from two species of banana slugs (*Ariolimax californicus* Cooper 1872 and *A. buttoni* Pilsbury and Vanatta 1896) collected in Santa Cruz and Fort Bragg, CA, respectively. The animals were kept in the laboratory, fed daily and remained well hydrated. All the subjects selected for the study maintained a constant mass throughout the entire study. All the experiments were performed at room temperature (20–22°C). The specimens used in this study covered a relatively wide range of mass (0.06–41.84 g), length (7–280 mm) and number of pedal waves (6–23).

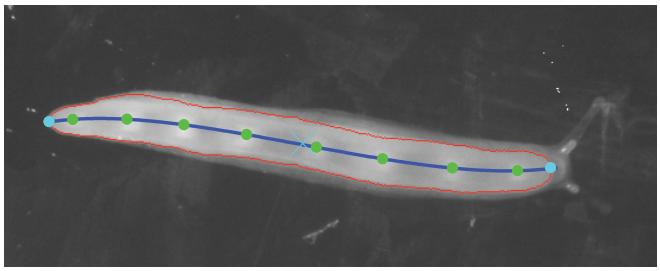

Fig. 3. The ventral foot surface of a moving garden slug. The outline of the ventral foot (red line), the location of the centroid of the animal's foot (blue X), its anterior and posterior ends (blue circles), the animal centerline (blue line) and the locations of each of the pedal waves (green circles) were determined using digital image processing.

Kinematics

In the set of experiments aimed at investigating the kinematics of motion, the animals were allowed to crawl freely on a horizontal, acrylic transparent surface. The pedal waves and the entire surface of the rim were visualized from below using appropriate lighting (Fig. 1). High-resolution (1024×1024 pixels), gray-level time-lapse image sequences of the animal's foot during steady locomotion were recorded at a rate of 30 frames s^{-1} for 3 to 6 s. A maximum of five locomotory events were recorded for each individual animal. We always measured the speed of the center of mass of the animal; the trials during which the animals were accelerating/decelerating and/or changing their direction of motion were excluded from the analysis.

The entire ventral surface of the animal was captured in each frame to measure the changes in speed and wavelength of the pedal waves as they progressed from the tail to the head. Using custom-programmed image-processing techniques in MATLAB (The MathWorks, Natick, MA, USA), we computed the location of the centroid of the animal's foot, its anterior and posterior ends, the centerline and the location of each of the pedal waves in each frame (Fig. 3). The speed, frequency (the number of waves generated at the tail per second) and wavelength (distance between consecutive waves) of the pedal waves were subsequently calculated and correlated to the crawling speed of the animal (assumed to be equal to the speed of the foot's centroid).

Motion of the foot in regions of muscular contraction and relaxation was also studied in detail through magnified time-lapse image sequences of the middle portion of the ventral foot surface of large banana slugs. The banana slugs studied here have numerous visible speckles distributed across the ventral surface of their foot, enabling clear visualization of the motion of the wave, interwave and rim regions. These speckles varied slightly in size but were ~50 μm in diameter. As the slugs moved, we measured the velocity at each point of the rim, wave and interwave regions of the ventral foot by performing particle image velocimetry (Willert and Gharib, 1991) of the speckles using Insight™ software (TSI, Shoreview,

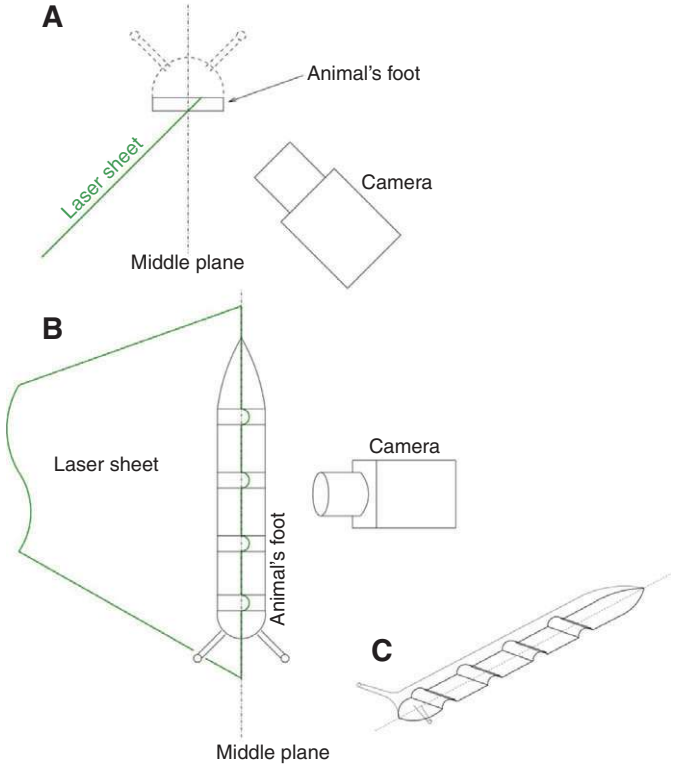

Fig. 4. (A) Front view of the experimental set-up. The animal is moving out of the page. (B) Top view of the experimental set-up. The animal is seen from above. (C) Three-dimensional sketch of a model animal. In the experiments, the animal was crawling over a thin glass plate, which is not shown here for clarity.

MN, USA). To obtain a more precise trajectory of the ventral surface across a wave, selected individual speckles were tracked manually and the corresponding velocity and acceleration were calculated.

In addition to the motion of the foot in the horizontal plane, we also measured the vertical displacements of the foot associated with the passage of each pedal wave. The animal's foot was illuminated from below with a laser sheet that formed a finite angle with respect to its vertical middle plane, as shown in Fig. 4. If the foot were a flat surface, the intersection of the laser sheet with the foot [hereafter the intersection line (IL)] would be straight and, therefore, its image would be a straight line in any camera view regardless of the pointing angle of the camera. However, if the foot was not flat, its intersection with the laser sheet would not be a straight line. Therefore, by properly choosing the pointing angle of the camera, one can observe IL deviations with respect to a straight line. Using simple geometrical arguments, it can be shown that the projection of these deviations on the image plane is proportional to the actual elevation of the foot with respect to the ground. In order to relate IL deviations measured in the image to vertical distances, a rectangular block with several notches of known depths was used as a calibration model. After each experiment, an image of the face containing the notches was acquired without changing the experimental setup to obtain the calibration factor, C (μm of vertical displacement per pixel).

Because the curvature of IL was not apparent to the naked eye, owing to the small value of the vertical displacements compared with the thickness of the laser sheet (Fig. 5), the curvature of the IL was quantified by measuring the displacements of the points of maximum brightness corresponding to two image strips in a time-

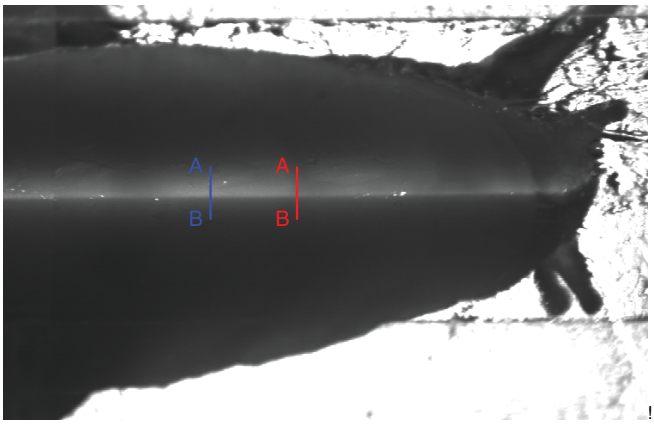

Fig. 5. Image of a garden snail's foot illuminated by the laser sheet. In this example, both the laser sheet and the camera's pointing direction formed an angle of ~20 deg with respect to the symmetry plane of the animal. The blue and red lines are image lines whose gray-level curves (shown in Fig. 6) were to be correlated. A add B denote the origin and end, respectively, of the strips whose gray level is plotted in Fig. 6.

lapse sequence, as illustrated in Fig. 5. These strips were placed far enough apart to guarantee that while a pedal wave passes over one of them, the other is at the interwave. The gray levels of the image along these two lines were fitted to Gaussian models after subtracting the background illumination (Fig. 6). The distance between the points of maximum brightness of both fitted lines was used to qualify the relative vertical displacement.

Dynamics

Previous studies measured the propulsive and friction forces under the gastropod foot using a discrete force balance located at various points on the substrate (Denny, 1981; Lissmann, 1945b). These force measurements were strictly one-dimensional and were obtained either underneath a small portion of the foot using a force plate mounted vertically at an instant of time (Denny, 1980a) or integrated over a large area of the foot of the animal with a force plate mounted horizontally (Lissmann, 1945b). In our study, we obtained time series of high-resolution measurements of the spatial distribution of two-dimensional forces under the entire foot of the animal using

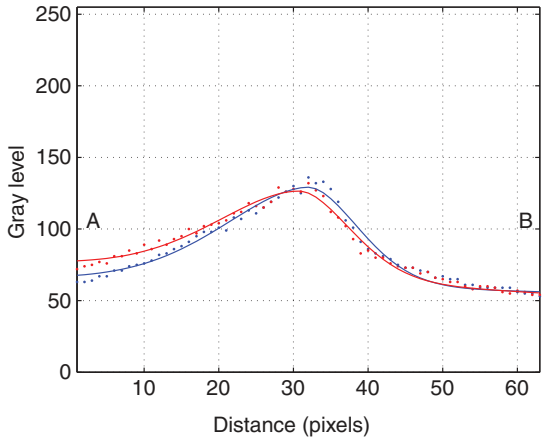

Fig. 6. Gray-level curves along the two image lines shown in Fig. 5. A and B correspond to the upper and lower parts of the image lines in Fig. 5. Dots represent actual gray-level values whereas solid lines are the result of fitting a Gaussian model to the gray level once the background illumination was subtracted.

a method that was initially developed in our laboratory to study the dynamics of cell migration (del Alamo et al., 2007). This traction cytometry method consists of measuring the deformation of a flat elastic substrate on which the animal is crawling. The mapping of the force field produced by the animal is then obtained from the measured deformations by solving the elastostatic equation at each time step [for details of the method, see the supplementary information in del Alamo et al. (del Alamo et al., 2007)] (Meili et al., 2010).

In each experiment, the animal was placed on an elastic gelatin substrate that was embedded with silver-coated, hollow glass spheres acting as marker beads. To fabricate the gelatin substrate, Nabisco Knox gelatin (3.4% w/v) was added to boiling water and stirred until completely dissolved. Silver-coated, hollow glass marker beads 10 μm in diameter were added to the gelatin solution, and the gelatin–marker-bead mixture was poured into glass Petri dishes (90 mm diameter). The gelatin solution was stirred and allowed to cool at room temperature for 30 min before refrigeration, ensuring that the marker beads were distributed evenly near the surface of the gel. The solution was then refrigerated at 4°C for 8 h. The gel was re-warmed to room temperature for 30 min prior to performing each experiment, avoiding water condensation on the outside of the Petri dish. The gelatin substrates used in all the experiments reported here had a mean thickness (h) of 8 mm and a mean (±s.d.) elastic modulus of 3159±678 Pa at room temperature. This value was about ten times larger than the shear stresses measured in the experiments, so that gelatin could be considered as a stiff substrate as a first approximation. This is an important point because it ensured that the behavior of the animal crawling on gelatin was nearly the same as when crawling on stiff substrates such as hard acrylic or glass.

The animal was placed on the surface of the gel and allowed to move freely. When crawling over the gel, the animal exerted stresses on the elastic substrate, causing its deformation. The horizontal deformation field at a constant depth (h_0) (100 μm beneath the surface, h_0=7.9 mm; Fig. 7) of the substrate was then obtained by measuring the displacement of the marker beads relative to their resting position. The resting position of the beads was recorded in the absence of the animal at the beginning and end of each experiment. Comparison of the initial and final positions of the marker beads was routinely performed to ensure that the gel always behaved as a perfectly elastic material in the range of deformations of interest, returning to its original state once the stresses ceased.

A schematic of the experimental set-up is shown in Fig. 7. The marker beads were illuminated by a thin horizontal laser sheet of 200 μm thickness. A charge-coupled device (CCD) camera was located directly underneath and focused at 100 μm beneath the surface of the substrate. The depth of field of the camera was ~10 μm. The two-dimensional shear stress field on the surface of the substrate was then calculated from the deformation of the gel (measured every 1/15 s) using an explicit analytical solution to the equation of static elastic equilibrium derived by del Alamo et al. (del Alamo et al., 2007). This method accounts for the finite thickness of the elastic substrate, which is crucial to the accuracy of the measured forces when this thickness is comparable to or smaller than the length of the animal, as was the case in all our experiments. From the measured shear stress field, the propulsive forces generated under the interwaves (the stationary part of the foot) as well as the sliding friction under the rim and the waves (portions of the sole surface that are moving forward) were calculated at each time point.

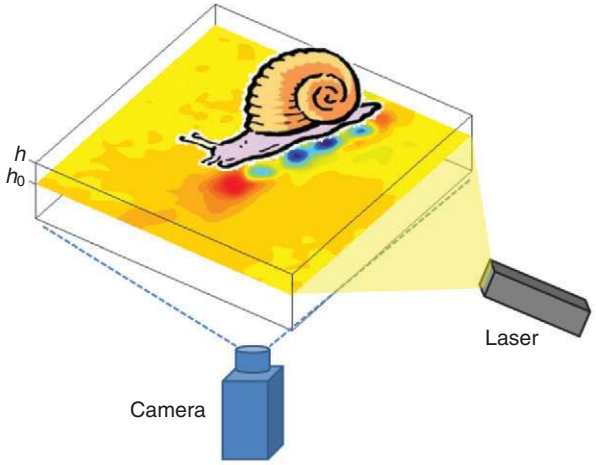

Fig. 7. Schematic of the experimental set-up. As the animal crawled on the gelatin substrate (thickness h=8 mm), the deformation of the gel was measured by tracing the displacement of the embedded marker beads, which were illuminated by the planar laser sheet (h_0=7.9 mm). Time-lapse images (15 frames s^{-1}) of the illuminated laser plane were recorded. The deformation vector at each point was calculated by applying correlation techniques.

In order to determine if unsteady inertial effects had to be considered in the determination of the propulsive stresses, we estimated the order of magnitude of all the terms in the equations of motion of the gel (see Appendix 1). Based on this order-of-magnitude analysis, we concluded that the inertial effects were typically 10^4 times smaller than the elastic stresses produced by the spatial deformations in all our experiments, thereby demonstrating that the elastostatic equation and method developed by del Alamo et al. (del Alamo et al., 2007) can be used to accurately measure the propulsive stresses exerted by all the migrating gastropods reported here. At the end of each experiment, the stiffness of the gelatin (modulus of elasticity) was calculated by measuring the static deformation produced by a metal sphere of known diameter and density placed on the surface of the gelatin (Keer, 1964).

It should be noted that the analytical solution of the elastostatic equation used to calculate the propulsive forces employs Fourier expansions and, therefore, requires the measured deformations to be spatially periodic. We satisfied this requirement in our experiments by placing the animal at the center of the recorded field of view such that, when the animal moved and applied the propulsive stresses, the deformations decayed to zero at the edges of the field of view. Therefore, to ensure accurate force calculations, the length and width of the field of view were chosen in each experiment to be a multiple of the length of the animal. This condition restricted our force measurements to small garden slugs and garden snails, 7 to 40 mm in length, with a maximum of eight pedal waves occurring at each time point.

Because the displacement of the vertical beads could not be extracted from the acquired images, the calculation of the propulsive stresses was performed under the assumption that the animal exerts negligible normal stresses at the free surface. This assumption led to errors in the obtained stresses because the weight of the animal acted as a normal stress on the surface of the substrate. However, these errors were estimated and shown to be negligibly small for all the animals included in the stress measurements presented here (0.2–1.6 g in mass) (see Appendix 2). All the measurements

Table 1. Mean (±s.d.) area ratios of the rim, interwaves and waves over the ventral foot surface and range of mass for the gray garden slug, banana slug and garden snail

Species	Number of animals	Rim/total area (%)	Interwaves/total area (%)	Waves/total area (%)	Range of mass (g)
Gray garden slug (*Deroceras reticulatum*)	20	54.17±2.78	33.62±2.85	12.21±2.1	0.06–0.52
Banana slug (*Ariolimax californicus*, *A. buttoni*)	8	52.47±2.13	30.56±2.37	16.97±2.06	3.26–41.84
Garden snail (*Helix aspersa*)	8	40.18±1.85	42.23±2.76	17.59±1.78	0.35–7.77

regarding the dynamics – including substrate deformation, stresses and traction forces – were in the horizontal plane and reported in two directions, either along (tangential) or perpendicular (transversal) to the motion of the animal on that plane.

Statistical analysis

All statistical analysis was performed in MATLAB (Version 7.4). Linear least-squares regression was used to model the relationship between the following pairs of variables: (a) crawling speed and wave frequency, (b) crawling speed and wavelength and (c) traction force (normalized to animal weight) and crawling speed. The Pearson correlation coefficient (ρ) was determined and statistical significance was set at $P<0.05$ to reject the null hypothesis ($\rho=0$) that no correlation exists between the pairs of variables.

RESULTS

Kinematics

Overall movement of the ventral surface

The foot of a crawling slug or snail is characterized by three distinct regions: the waves, the interwaves and the rim (supplementary material Movie 1). For the direct, monotaxic-wave gastropods studied here, the waves propagate from the posterior to the anterior ends of the animal along the length of the foot, whereas the interwaves remain stationary in the laboratory reference frame. This wave train is surrounded laterally by flat regions (the rim) that move forward at the speed of the center of mass. The constant speed of the center of mass is considerably slower than that of the waves. The mean area ratios occupied by the rim, interwaves and waves over the entire foot area measured in steadily crawling banana slugs, garden slugs and garden snails are shown in Table 1. The rim region occupied >50% of the ventral surface in garden slugs and banana slugs. In general, the wave trains on the ventral surface of garden snails appeared to be wider compared to those observed in slugs, resulting in a smaller rim area ratio (40.18±1.85%). The mean area ratios of the pedal waves over the total ventral surface ranged from 12.21 to 17.59% in all of the gastropods examined. The ranges of mass of these animals are also reported in Table 1.

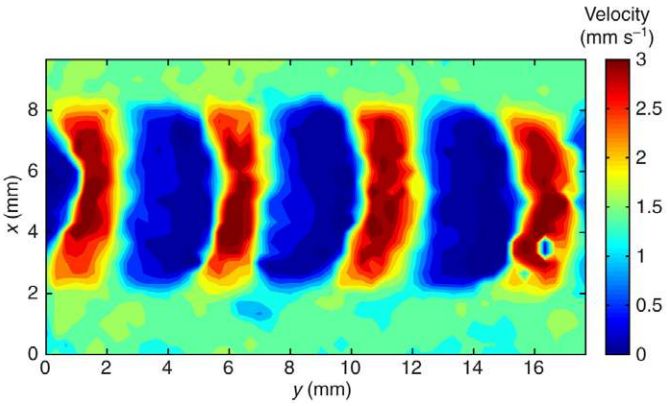

Fig. 8. The foot of a crawling gastropod is characterized by three distinct regions (waves, interwaves and the rim), as shown in this velocity contour map of a portion of the ventral surface of a banana slug (~20% of the length of the animal is shown). The velocity was measured along the direction of motion of the slug and in the laboratory reference frame (zero velocity means that the animal is stationary with respect to the substrate). The waves (red D-shaped regions), interwaves (blue D-shaped regions) and rim (pale green/yellow regions flanking the waves and interwaves) can be distinguished by their distinct velocity magnitudes. Notice that the velocity dropped to zero behind each wave and increased abruptly upon reaching the wave region. The blue patch of low-velocity regions on the lower right portion of the first wave from the right was caused by hardened mucus left by the slug during previous trials.

The rim, interwave and waves can be clearly identified based on their distinct velocities, as illustrated in Fig. 8. On the ventral foot surface, waves of muscular contraction appeared as D-shaped regions that move faster than the rest of the surface (red regions in Fig. 8). Consecutive high-velocity regions of muscular contraction were separated by D-shaped, dark blue regions (zero velocity with respect to the substrate), which correspond to the interwave regions of muscular relaxation. The train of waves and interwaves was surrounded by the rim (pale green/yellow in the upper and lower portions of Fig. 8), which had a nearly constant velocity that was equal to the crawling speed of the animal (defined as the velocity of the centroid of the foot).

The velocity profile of the ventral surface was not symmetric across each pedal wave. Fig. 9 shows the measured displacement of a representative speckle on the ventral foot surface of a banana slug as a wave passes over it (Fig. 9A), as well as the calculated velocity and acceleration over a period of ~1 s (Fig. 9B and 9C, respectively). The speckle was stationary before (<0.2 s) and after (>0.8 s) a wave passed over it. As a wave approached it, the speed of the speckle gradually increased, reached a maximum value and then decreased rapidly to zero after the wave passed (Fig. 9B). The velocity of the foot along the wave was not symmetric and the period over which acceleration occurred was approximately twice that of deceleration. The acceleration from zero to maximum velocity (3.28 mm s^{-1}) occurred relatively smoothly whereas the deceleration (maximum deceleration ~14 mm s^{-2}) of the velocity to zero happened abruptly.

Pedal wave kinematics

The kinematics of the pedal waves, including changes in wavelength and wave frequency, in relation to the overall crawling speed was investigated. Fig. 10 shows the dependence of crawling speed on the wave frequency (Fig. 10A) and mean wavelength (Fig. 10B) measured in 45 locomotor events for 22 individual garden slugs. The overall crawling speed correlated positively with the mean wavelength as well as wave frequency ($P<0.05$; Fig. 10A,B).

We observed complex patterns of pedal wave propagation along the foot of all of the gastropod species crawling at constant speeds. In the case of garden snails, loping waves appeared frequently in addition to the forward-propagating pedal waves (note that the

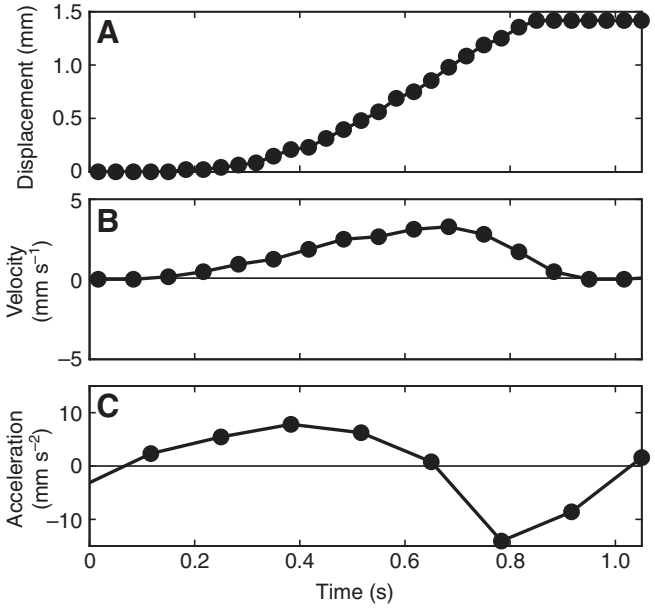

Fig. 9. Representative patterns of (A) forward displacement, (B) the corresponding velocity and (C) the acceleration of the foot of a banana slug during the passage of a pedal wave. The velocity profile indicated that the wave geometry was not symmetric, showing slow acceleration at the posterior half of the wave and a more abrupt deceleration at the anterior half.

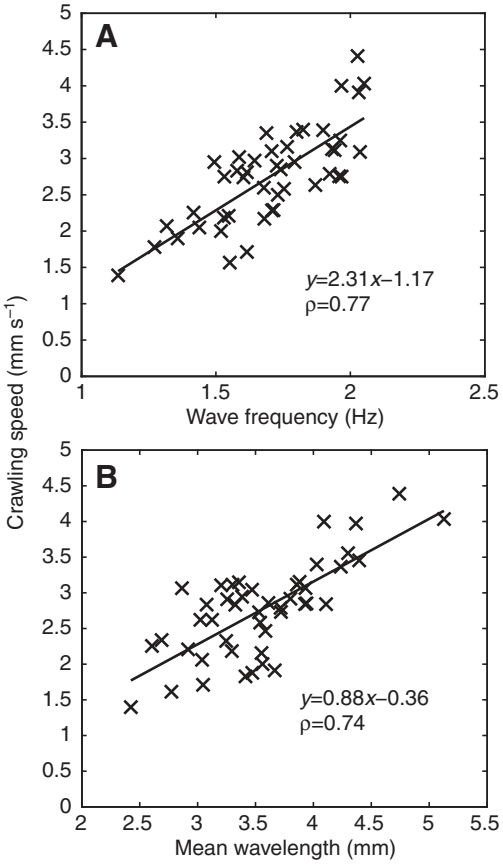

Fig. 10. The overall crawling speed of garden slugs correlated positively with (A) wave frequency (P<0.05) and (B) wavelength (P<0.05). Each data point was obtained by averaging the crawling speed and wavelength of an individual slug over a locomotor event of 3–6 s (N=45 runs, 22 animals).

animals that exhibited this dual mode of locomotion are not considered here). In garden slugs and banana slugs, wave propagation exhibited distinct variations along the ventral surface, characterized by a dependence of the wave speed and wavelength on the position along the animal's foot. Fig. 11 shows measurements of the pedal wave speed along the ventral surface of 15 garden slugs (25 locomotory events) and four banana slugs (eight locomotory events). Although there was some level of variability, the data clearly showed that in both species the propagation speed of pedal waves was not constant, as was reported by Crozier and Pilz (Crozier and Pilz, 1924). The wavelength and speed increased steadily with the distance to their origin (the tail of the animal) and peaked near the head. The variations in wave speed with respect to the animal's centroid along the foot were considerable and the maximal wave speeds were 2.61±0.44 and 4.54±1.68 times the animal's crawling speed in garden slugs and banana slugs, respectively (mean crawling speeds were 2.49±1.68 mm s^{-1} in garden slugs and 1.57±0.43 mm s^{-1} in banana slugs). The ratio between peak speed of the pedal waves and the velocity of the animal's centroid increased with the number of waves observed on the ventral foot of the animal. Pedal waves accelerated more in banana slugs (with >20 waves) than in the smaller garden slugs (with 7–8 waves), reaching speeds up to almost five times the speed of the animal.

Most of the wave-propagation patterns we observed coincided with the average pattern shown in Fig. 11. However, we also observed other, less-frequent wave propagation patterns. The wave configurations observed in all our experiments can be classified into three groups: (1) acceleration of pedal waves described above (Fig. 12A,D,G), (2) symmetric acceleration and deceleration (Fig. 12B,E,H) and (3) rapid acceleration–constant speed–rapid deceleration (Fig. 12C,F,I). Representative measurements from three individual garden slugs of comparable sizes exhibiting these three wave configurations are plotted in Fig. 12. Fig. 12A–C shows the distance traveled by each wave from its origin at the tail of the animal as time progressed, together with the corresponding distance traveled by the centroid of the animal's foot. From these trajectories, we calculated the wavelength of the pedal waves (Fig. 12D–F) as the distance between two consecutive waves and the wave speeds (Fig. 12G–I) as the local slope of the trajectories.

In the most commonly observed wave pattern (Fig. 12A,D,G), the wavelength increased steadily with a constant acceleration as the pedal waves propagated from the posterior end and reached a maximum value after traveling ~80% of the animal's length ($x/L\approx0.8$, where x is the distance from the tail and L is the length of the animal). The wavelength then decayed rapidly back to its initial value as the wave approached the anterior end of the animal. This behavior was clearly observed in the animals shown in Figs 1 and 3. A similar pattern in wave speed was observed as the waves progressed along the foot, indicating that wave speed was modulated by the wavelength while the wave temporal frequency remained constant, as expected in steady motion. In the next, less-frequent pattern (Fig. 12C,F,I), constant wavelength and wave progression speed along a major portion of the foot were observed. Upon appearing at the posterior end of the foot, each wave quickly accelerated to a certain speed and remained constant as it progressed forward. As the wave approached the anterior end of the foot, it decelerated quickly to its original speed. Finally, the wavelength and wave speed occasionally increased and decreased symmetrically

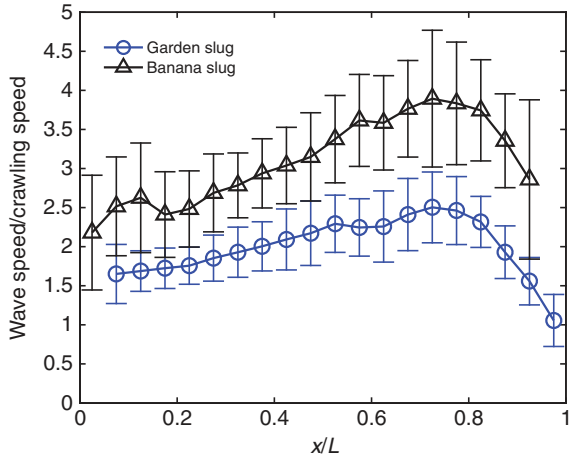

Fig. 11. The propagation speed of pedal waves in garden slugs and banana slugs varied substantially as the waves propagated along the animal. Wave speeds along the foot of banana slugs (black triangles) and small garden slugs (blue circles) are represented as a function of the distance from the tail of the animal, x, normalized by animal length, L (banana slugs: N=8 runs, 4 animals; garden slugs: N=25 runs, 15 animals). Data are presented as means ± s.d.

along the foot, reaching a maximum value near the center of the animal (x/L=0.5; Fig. 12B,E,H). This symmetric pattern was typically observed in animals with a relatively high crawling speed (>3 mm s^{-1}).

Note that in all cases the starting and ending velocities of the waves were identical and approximately equal to the crawling speed of the animal (wave speed/animal speed=1). The wave speed at locations very near both ends of the animals could not be measured owing to difficulties in identifying the exact location of the waves when they were very close to the rim (see Fig. 1). As a result, the measured normalized wave velocity shown in the figures (Fig. 11 and Fig. 12G–I) was not exactly one. Nevertheless, the speed of the wave should match that of the rim as there is no discontinuity in the ventral foot surface, so the normalized wave speed was expected to start off and end at unity (at x/L=0 and x/L=1).

Although three distinct wave propagation patterns were observed, constant wave acceleration along the animal (Fig. 11 and column 1, Fig. 12) was clearly the most prevalent pedal wave pattern, as it was observed in >60% of the total number of individual animals tested. The statistical distribution of the wave-speed patterns in small garden slugs and banana slugs is shown in Fig. 13. This figure contains data from 22 garden slugs and six banana slugs in 41 and 12 steady-speed crawling trials, respectively. No more than three trials from each animal were included in this analysis and the number of wave propagation patterns observed in multiple trials of an individual animal was normalized by the total number of trials conducted in that individual.

Vertical displacements of the foot

Vertical displacements of the foot were measured during the passage of muscular contractions and relaxations. Fig. 14 shows the time evolution of the vertical displacements between two locations on the foot corresponding to the blue and red lines shown in Fig. 5. The periodicity of the vertical displacements was ~0.5 s, which corresponded well to the pedal wave periodicity obtained by visual inspection of the time-lapse image sequence (0.56 s).

The calibration performed after the experiment yielded a calibration factor of 67 μm pixel^{-1}. Based on measurements of the

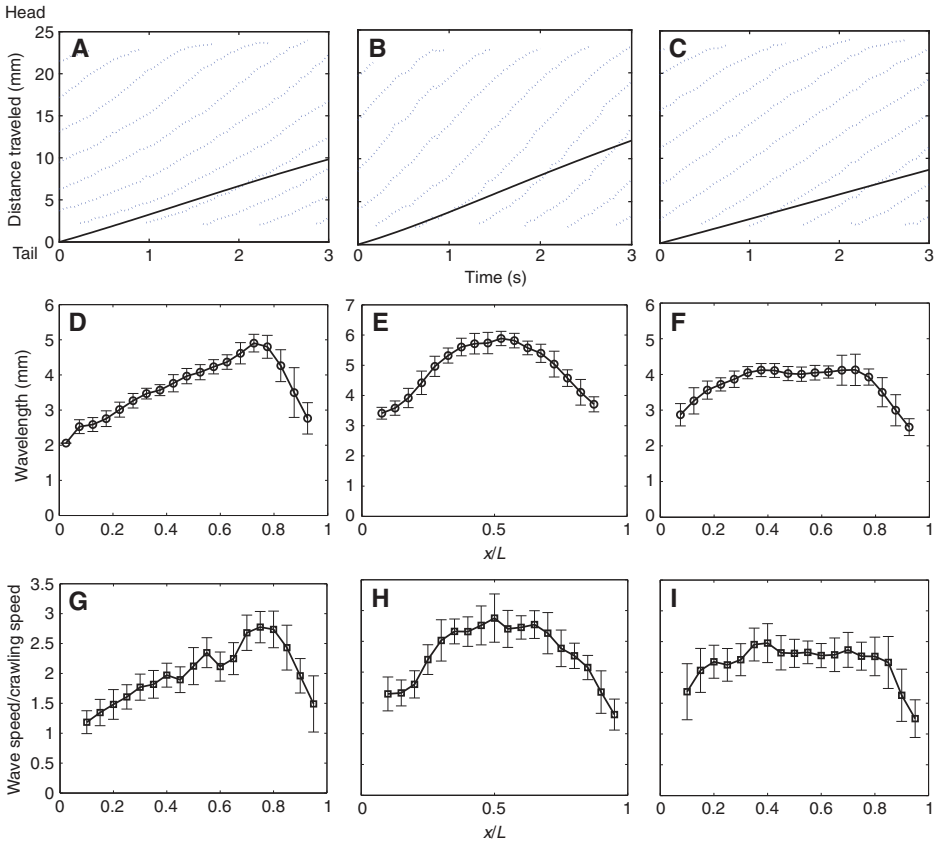

Fig. 12. Representative patterns of wave propagation in garden slugs. (A–C) Time evolution of the displacement of the waves (dotted lines) compared with the overall displacement of the centroid of the animal (solid black lines), (D–F) wavelength variation along the animal's foot represented as the distance from the tail normalized by the length of the animal, x/L (means ± s.d.) and (G–I) wave speed along the animal's foot normalized by the speed of the crawling and represented as a function of x/L (means ± s.d.). Three wave-progression patterns were identified: (1) acceleration of pedal waves (A,D,G), (2) symmetric acceleration and deceleration (B,E,H) and (3) constant wave speed along the animal (C,F,I). Each column represents data collected from an individual garden slug.

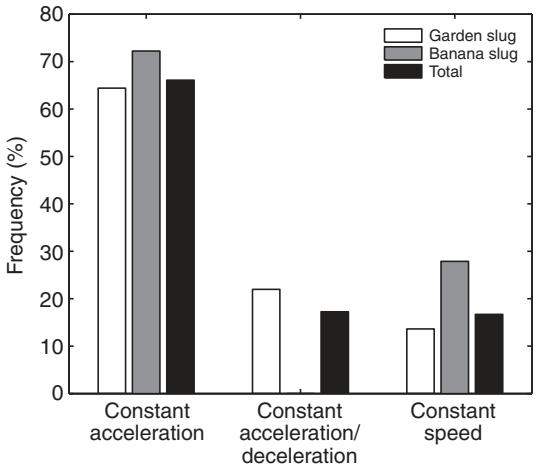

Fig. 13. Percentage distribution of the three wave propagation patterns shown in Fig. 9. Data are from 22 garden slugs and six banana slugs in 41 and 12 steady-speed crawling trials, respectively. In both species, acceleration of pedal waves occurred in >60% of the runs.

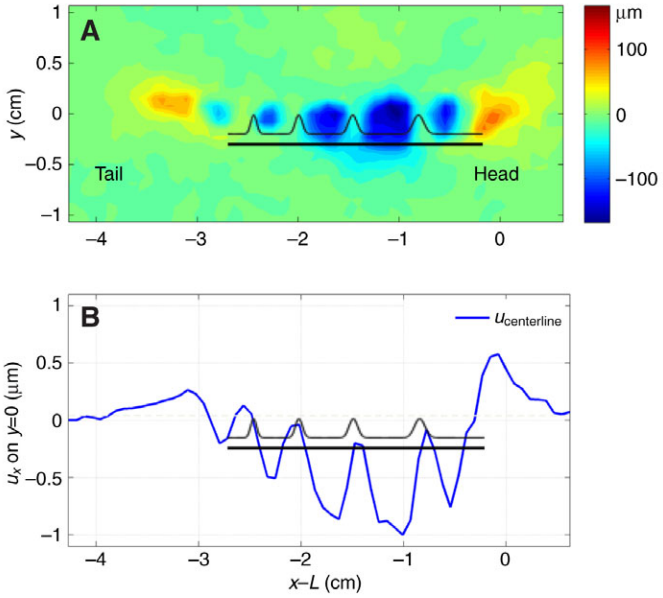

Fig. 15. Deformation generated by a moving garden snail on the surface of the substrate in the animal's direction of motion (longitudinal). (A) Two-dimensional contour map of the longitudinal deformation as a function of the longitudinal (x) and transversal (y) spatial coordinates. Red, the animal is deforming the gel towards the right of the panel underneath the head and tail; blue, the animal is deforming the gel towards the left of the panel under the interwaves. (B) Longitudinal deformation along the centerline of the ventral foot ($u_{centerline}$) as a function of x. In both panels, the origin of the coordinate system is located at the intersection between the centerline of the ventral foot and the head of the animal. The black undulating pattern and the black horizontal line have been included to indicate the position of the waves and interwaves relative to the peaks and valleys of the deformation field.

oscillations in the distance between the locations of maximum brightness, we concluded that the vertical displacement of the animal's foot was ~70 μm (≈1 pixel). The sign of such displacement can also be determined by joint examination of the displacement *vs* time curve (Fig. 14) and time-lapse images. Experiments performed for different animals yielded similar displacement values, with vertical displacements up to 80 μm.

Dynamics

Substrate deformation caused by a moving gastropod reflected the regional variations in the ventral surface movement (Fig. 15). During steady locomotion, the muscular foot of the animal pushed the substrate backwards in each of the interwave regions (blue regions in Fig. 15). By contrast, the animal pulled the substrate forwards beneath its tail and head (yellow regions in Fig. 15). This deformation pattern was observed consistently in both garden slugs and snails (Fig. 16A,B). Interestingly, the magnitude of substrate deformation was modulated by the distance between the pedal waves, reaching maximum levels beneath the stationary interwaves and minimum levels beneath the waves. Each pedal interwave produced backward-directed stresses along the direction of motion whereas forward-directed stresses were imposed on the substrate underneath the regions occupied by the rim, the pedal waves and the anterior and posterior ends of the animal (Fig. 16C,D). The spatial organization of longitudinal stresses on the ventral foot surface is depicted in Fig. 17A. By invoking Newton's third law, we expect that similar stresses were exerted along the opposite direction on the animal's foot. As a result, the foot surface experienced a forward push on the stationary interwaves and a backward drag on the forward-moving waves and rim.

The horizontal stresses perpendicular to the direction of motion formed a train of paired patterns of opposite signs (Fig. 16E,F). These stress patterns appeared in the regions of the substrate underneath the interwaves, indicating that these areas were pushed inwards toward the centerline of the animal in addition to being pushed backwards along the direction of motion. Although the substrate deformation reached positive peaks beneath the head and tail of the animal, it always remained negative beneath the waves and interwaves. This spatial organization is depicted in Fig. 17B.

Overall, the horizontal stress distribution along the direction of motion (Fig. 18) exhibited periodic patterns similar to that of the deformation (Fig. 15), with periodic positive (forward) peaks beneath the waves and negative (backward) peaks in the interwaves. The maximum stress magnitude beneath the interwaves was significantly higher than that in the wave and rim regions. The ratios between the maximum stress magnitudes beneath the interwave regions and

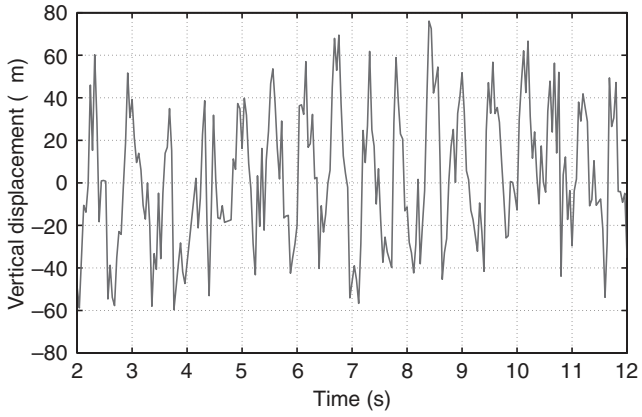

Fig. 14. Relative vertical displacement of the foot between the locations corresponding to the blue and red lines shown in Fig. 5.

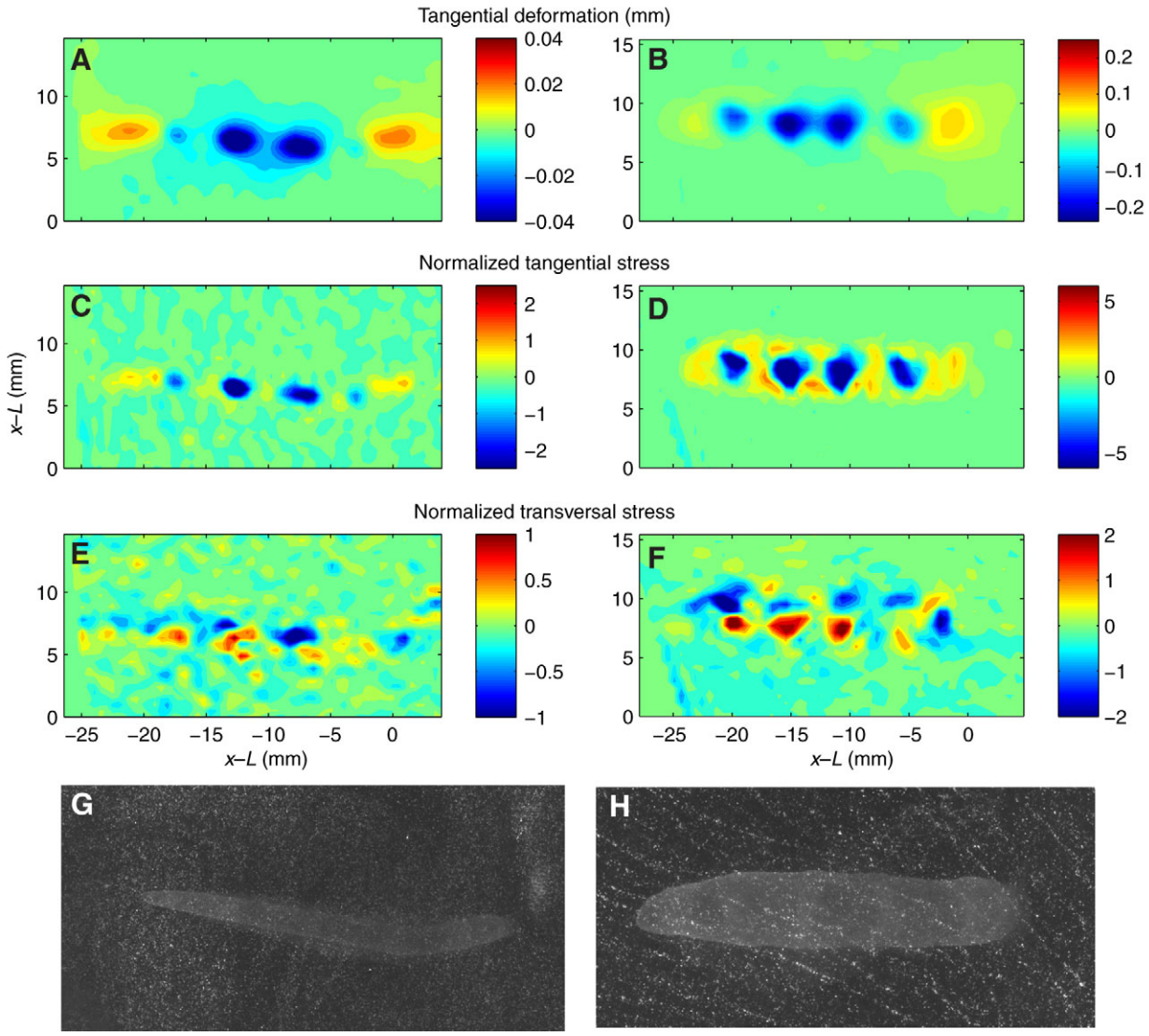

Fig. 16. Spatial distribution of the propulsive stresses generated by two terrestrial gastropods while crawling on a gelatin substrate. The data in the left column are from a garden slug and the data in the right column are from a garden snail. (A,B) Contour maps of substrate deformation in the animal's direction of motion. (C,D) Contour maps of horizontal stresses in the direction of motion. These stresses were normalized with the normal stresses caused by the animal's weight (estimated to be spatially uniform and equal to the ratio of the animal weight to the area of the foot). (E,F) Contour maps of horizontal stresses in the direction perpendicular to the motion. (G,H) Brightness images showing the ventral foot of each animal and the marker beads used to measure the propulsive stresses. In both images, the animals were crawling from the left to the right.

the wave regions were 2.39±0.297 and 2.35±0.52 for garden snails (N=7 runs, 3 animals) and slugs (N=3 runs, 2 animals), respectively.

The net propulsive force generated by the pedal waves of an animal in steady-speed motion considered here was offset by the viscous shear forces of the rim and waves, which can be calculated by integrating the stress beneath the interwaves. In spite of the complex stress patterns generated beneath the animal's ventral foot surface, the net forward force was found to balance the sum of the backward shear forces produced by the forward-moving waves and the rim. The calculated propulsive forces were normalized by the weight of the animal in order to compare the propulsive forces for animals of different weight. For garden snails, there was a trend of increasing normalized propulsive force with increasing crawling speed (Fig. 19), although this trend was not statistically significant (P=0.32). For the garden slug, however, there was no clear correlation between normalized propulsive force and crawling speed, possibly owing to the limited spatial resolution of our stress measurements in this case. Because the width-to-length ratio of a garden slug's foot is smaller than that of a garden snail, the fine-scale details of the slug's stress distributions could not be captured as precisely as the garden snail's, resulting in less accurate, resultant propulsive forces.

DISCUSSION

The ventral surface of a locomoting terrestrial gastropod is characterized by a train of alternating pedal wave and interwave regions that propagates from tail to head. The interwaves are stationary with respect to the ground whereas the waves move faster than the animal. The wave train is surrounded by a continuous rim that moves at the velocity of the animal (Fig. 1). Overall, the motion of the ventral surface observed in this study was in agreement with

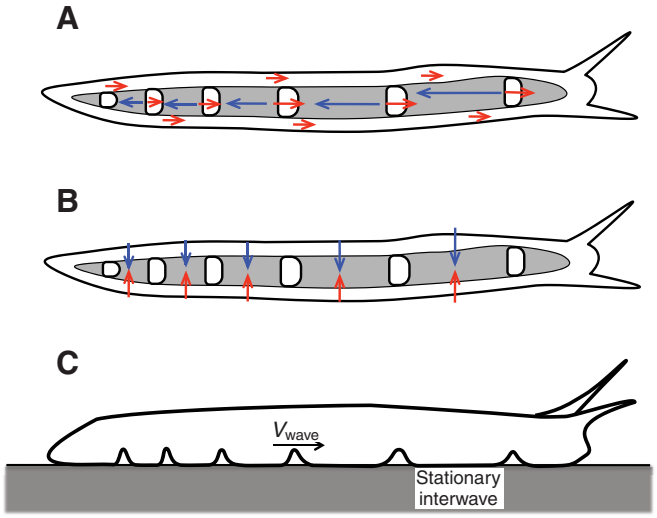

Fig. 17. Sketch of the spatial organization of the horizontal stresses exerted by terrestrial gastropods on a substrate. (A) Stresses in the direction of motion (plan view). (B) Stresses in the direction normal to motion (plan view). (C) Side view of the animal. V_{wave}, speed of the pedal waves.

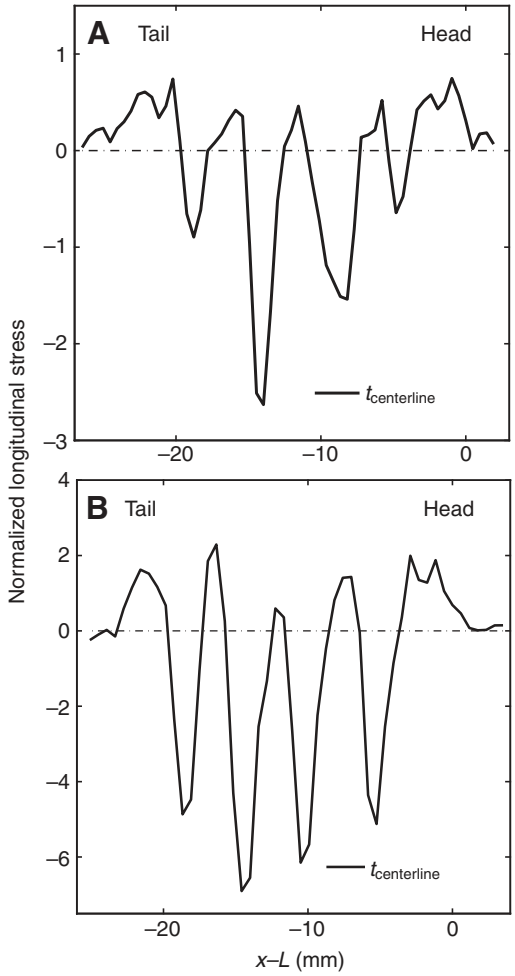

Fig. 18. Horizontal stresses generated by the animals shown in Figs 12 and 16 along their direction of motion, measured along the centerline of their ventral feet ($t_{centerline}$) and represented as a function of the distance to their heads. (A) Garden slug in panels A, C and E of Fig. 12; (B) garden snail in panels B, D and F of Fig. 16. Stresses were normalized by the vertical stresses produced by the animal's weight in order to allow comparison between animals. Stress oscillated from positive to negative peaks along the animal, indicating regions of waves and interwaves, respectively. In both animals, the stress magnitudes of the interwave regions (negative peaks) were significantly higher than those of the pedal wave regions (positive peaks). Dot–dash lines indicate the baseline, zero stress level.

previous studies (Crozier and Pilz, 1924; Denny, 1981; Jones, 1973; Lissmann, 1945a; Lissmann, 1945b; Parker, 1911). However, close examination of our high-resolution measurements revealed that the spatiotemporal organization of both pedal waves and interwaves is more complex than had been previously assumed. The waves are not symmetric (Fig. 9), nor do they move at a constant speed (Fig. 11). Previous studies considered that pedal waves are symmetric and that both their length and propagation velocity are constant. Consistent with the premise of constant pedal wave properties, Denny also assumed that there is no pressure build-up between consecutive waves (Denny, 1981). It appears that recent mathematical models on the propulsion mechanics of adhesive crawlers have relied on most of these assumptions (Chan et al., 2005; Lauga and Hosoi, 2006).

Our measurements of the motion of speckles on the surface of the ventral foot revealed asymmetric displacement pulses during the passage of each wave. Furthermore, the waves themselves were found to deform and accelerate as they progressed from the posterior to the anterior end of small garden slugs and banana slugs. Among the different wave-propagation patterns that were observed, steady wave acceleration (lengthening of the wavelength) followed by abrupt deceleration (shortening of the wavelength) was clearly predominant. Our traction measurements clearly showed that the variable speed of the pedal waves modulated the magnitude of the stresses under each wave. The pedal wave asymmetry and acceleration we observed are two potential contributors to the locomotion of terrestrial gastropods that have not been considered previously and warrant exploration in future modeling efforts. In fact, the observation that steady wave acceleration was present in two species that differ widely in size, such as garden slugs and banana slugs, suggests that this pattern is mechanically relevant to the locomotion of the animal.

Two-dimensional substrate deformation and stresses generated by the ventral foot surface elucidated the mechanical role of the pedal waves in pedal force generation. A net forward force was generated beneath each stationary interwave, where the animal pressed its foot against the substrate and pulled it backwards (Fig. 16). The sum of the propulsive forces generated under the interwaves was shown to balance the sliding friction caused by the forward-moving waves and the continued translation of the rim, head and tail of the animal. Moreover, the magnitude of the horizontal stresses along the direction of motion was considerably higher under the interwaves than under the waves. This result is consistent with the rheological properties of the mucus measured by Denny for *A. columbianus* (Denny, 1980a). Denny's measurements showed that, when the shear stress acting on the mucus exceeds the yield stress, it starts flowing and the stress required to maintain a given strain rate drops to approximately half the yield stress. Furthermore, it should be pointed out that the stress-strain rate curve of the mucus is monotonically increasing; thus, if the foot is flat and the wave does not lift, one would expect the stresses under the fast-moving pedal wave to exceed those under the slower rim.

The fact that the magnitude of the shear stresses underneath the pedal wave was comparable with that under the rim supported the

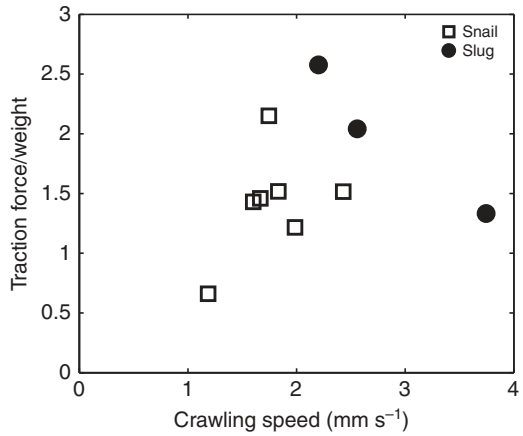

Fig. 19. Relationship between normalized traction force (traction force/animal weight) and crawling speed of the animal. Open squares represent data from garden snails (*N*=7 runs, 3 animals) and filled circles represent data from garden slugs (*N*=3 runs, 2 animals). Although a trend of increasing normalized traction force with increase in crawling speed was observed in snails, this trend was not statistically significant (*P*=0.32). For garden slugs, there was no clear correlation between normalized traction force and crawling speed, possibly owing to the limited spatial resolution.

observation that the foot was lifted under the pedal waves. The measured depth of the concavity of the pedal wave was small compared with the length of the wave (≈70 μm *versus* 5 mm in garden snails), which would explain why several authors were unable to measure these small vertical displacements. However, this depth was nearly an order of magnitude larger than the value reported by Denny and Gosline (Denny, 1981; Denny and Gosline, 1980) for the mucus thickness under the interwaves, 10–20 μm, which makes it plausible that pedal wave lifting plays a role in the locomotion.

The tangential stresses perpendicular to the direction of motion also exhibited an interesting pattern, with coupled stresses of opposite signs appearing in the interwave regions (Fig. 16E,F). It is possible that they were caused by the inward muscle contractions of the rim. Nevertheless, the role of this inward contraction in the generation of thrust remains unclear. We can only speculate that terrestrial gastropods might use these inward contractions to modulate substrate adhesion at the interwaves through the finite yield stress of the mucus.

It is worth mentioning that the magnitude of the horizontal stresses along the direction of motion generated by the pedal waves and interwaves was nearly one order of magnitude larger than the vertical stresses generated by the weight of the animal (Fig. 16C,D). This result has two implications. The first is that the errors introduced by the assumption of zero vertical stresses are negligible (see Appendix 2 for more details). The second is that terrestrial gastropods should be able to move up or down slopes by implementing pedal wave patterns similar to those reported here for translocation over flat surfaces. In fact, Denny showed that the frequency of the pedal waves was conserved when *A. columbianus* crawled vertically, either upwards or downwards, although the magnitude of the forces was higher for slugs crawling upwards (Denny, 1984).

It has been generally agreed that the overall crawling speed of a terrestrial gastropod correlates positively with the speed of the pedal waves (Crozier and Pilz, 1924; Denny, 1981; Jones, 1973; Jones, 1975). In particular, Jones reported that the overall crawling speed of a given animal is modulated solely by wave frequency (Jones, 1975). He also suggested that faster-moving species generally have more pedal waves on the ventral surface at all times than slower-moving species. We investigated the wave speed and frequency in relation to the overall crawling speed during steady locomotion in garden slugs. Consistent with previous studies, we found that the crawling speed increased with pedal wave frequency. Furthermore, we found a positive correlation between crawling speeds and mean wavelength, implying that the number of pedal waves present on the ventral surface of a given terrestrial gastropod decreased as the animal moved faster. Therefore, although longer animals generally have more pedal waves, the number of waves in a given animal decreased as it increased its crawling speed. From a mechanics point of view, a longer distance between pedal waves leads to a growth in the area ratio occupied by the interwaves, which could contribute to the higher propulsive force required for faster locomotion. The net propulsive forces generated by the interwaves were found to increase linearly with the animal's crawling speed, although this relationship was not statistically significant, possibly owing to the limited range of crawling speeds recorded.

There is little doubt that the rheological properties of pedal mucus are important for the locomotion of terrestrial gastropods. Strong experimental evidence supports the hypothesis that the viscoelastic nature of this mucus leads to the generation of asymmetric shear forces under the foot with a net forward component that propels the animal forwards (Denny, 1981; Denny and Gosline, 1980). Furthermore, a recent mathematical model has confirmed that the non-Newtonian nature of the pedal mucus can result in the generation of a net propulsive force when the waves are not lifted from the substrate (Lauga and Hosoi, 2006). Although Lauga and Hosoi clearly showed how the animal might take advantage of the rheological properties of the mucus, the mechanism they proposed relies on lubrication theory, thereby implying the existence of pressure gradients in the mucus along the pedal wave (Chan et al., 2005). However, our experiments (supplementary material Movies 2 and 3) showed that slugs were able to propel themselves over a mesh of very thin (<0.5 mm) parallel threads separated at a distance greater than the pedal wavelength without changing their pedal wave pattern or their frequency, which suggests that pressure variations beneath the foot are not essential to propulsion. Notice that a mechanism of stick-and-release, similar to the one used in caterpillars, is consistent with the yield-stress rheology of the mucus described by Denny (1980b). This mechanism would explain the ability of the animal to move on rugged, uneven terrain without forming a lubricating layer and is compatible with the measurements of shear stresses acting on the substrate discussed in this paper.

APPENDIX 1
Estimation of inertial effects in the calculation of pedal stresses

The pedal stresses produced by the animal on the surface of the gelatin substrate were determined by solving the equation of static equilibrium of the substrate. However, the passage of pedal waves along the animal's ventral foot surface led to rapid temporal accelerations of the substrate (10^{-4} m s^{-2}), which suggested that inertial effects might be important in the calculation of pedal stresses. Therefore, an order-of-magnitude analysis was performed to estimate inertial effects. The local form of the equation of motion for a body subjected to external load is:

$$\nabla \cdot \mathbf{T} + \rho\mathbf{B} = \rho\ddot{\mathbf{u}}, \quad \text{(A1)}$$

where $\mathbf{T}$ is the stress tensor, ρ is the mass density per unit volume, $\mathbf{B}$ is the body force per unit mass and $\ddot{\mathbf{u}}$ is the acceleration. Because

the gelatin substrate can be treated as a linear elastic isotropic body, we can use Hooke's constitutive relationship between stress and strain to arrive at the Navier equation, which, in the absence of body force (**B**=0), is written as:

$$(\Lambda + G)\,\nabla(\nabla \cdot \mathbf{u}) + G\nabla^2\mathbf{u} = \rho\ddot{\mathbf{u}}\,, \tag{A2}$$

where Λ and G are Lamé elastic parameters and **u** is the displacement vector. Based on our deformation measurements and the elastic properties of the gelatin substrate, an order-of-magnitude analysis can be performed to estimate the importance of the inertial term, $\rho\ddot{\mathbf{u}}$. For this purpose, we approximate Eqn A2 along the direction of the propagation of the pedal wave:

$$(\Lambda + G)\frac{u}{\lambda^2} + G\frac{u}{\lambda^2} \approx \rho u\omega^2\,, \tag{A3}$$

where λ is the wavelength of the pedal waves (distance between two consecutive waves), ω is their frequency and u is a typical value of the deformation of the substrate under each wave. To make a conservative estimate, we consider only the direction of wave propagation because changes in deformation rate occur most rapidly along this direction. A conservative estimate of the ratio between the inertial forces of the substrate (right-hand side of Eqn A3) and the elastic stresses (left-hand side of Eqn A3) is calculated using the following equation:

$$\frac{F_I}{\tau_E} = \frac{\rho}{G}(\lambda\omega)^2 = \frac{\rho}{G}c^2\,, \tag{A4}$$

where F_I is the inertial force, $\boldsymbol{\tau}_E$ is the elastic stress and $c=\lambda\omega$ is the speed of the pedal waves. In our experiments, $\rho \approx 103\,\mathrm{kg\,m^{-3}}$, $G \approx 103\,\mathrm{N\,m^{-3}}$ and $c \approx 10.2\,\mathrm{m\,s^{-1}}$. We can then estimate that the stresses due to inertial effects are typically 10^4 times smaller than the elastic stresses related to spatial deformation. As a result, the inertial effects were negligible and the elastostatic equation can be used to accurately calculate the pedal stresses exerted by the migrating gastropods on the substrate.

APPENDIX 2
Estimation of the effect of the weight of the animal on the measured pedal stresses

In this study, we obtained measurements of the whole spatial distribution of the propulsive and friction forces under the foot of moving gastropods. For this purpose, we placed the animals on an elastic gelatin substrate that was embedded with marker beads. As they moved, the propulsive and friction stresses produced by the animal deformed the substrate. We determined the horizontal deformation field at a constant depth of the substrate by measuring the displacement of the marker beads relative to their resting position. The two-dimensional shear stress field on the surface of the substrate was then calculated by solving the equation of static elastic equilibrium using Fourier expansions in the two horizontal directions, as described in del Alamo et al. (del Alamo et al., 2007).

The problem resulting from Fourier expansion of the elastostatic equation is an ordinary second-order equation involving three variables (the Fourier coefficients of the three components of the deformation field). This equation requires six boundary conditions to be specified at arbitrary vertical positions. It is straightforward to set three of these conditions by imposing zero deformations at the bottom of the substrate, where it is in contact with a rigid surface. Imposing the measured horizontal deformations on the measurement plane sets two more conditions. However, owing to the impossibility of measuring vertical deformations on the measurement plane within the current experimental facility, we could not set the sixth boundary condition using experimental measurements. Instead, we assumed that the normal vertical stresses on the surface of the substrate are equal to zero and used this assumption as a boundary condition.

Because the weight of the animal is supported by the substrate, the assumption of zero normal stresses on the surface of the substrate is not accurate in the region under the foot of the animal. If the Poisson ratio of the substrate is different than zero, the normal stresses generated by the weight of the animal cause horizontal displacements, which will be erroneously interpreted as coming from horizontal shear stresses by our force calculation method. To estimate the errors introduced by the assumption of zero normal stresses, we decomposed the real horizontal stresses as the sum of two contributions:

$$\boldsymbol{\tau} = \boldsymbol{\tau}(u,v,0) + \boldsymbol{\tau}(0,0,W)\,, \tag{A5}$$

where $\boldsymbol{\tau}(u,v,0)$ are the horizontal shear stresses caused by the measured horizontal deformations under zero normal stresses, $\boldsymbol{\tau}(0,0,W)$ are the horizontal shear stresses caused by a distribution of non-zero normal stresses such that the horizontal deformation on the measurement plane is zero and v is the horizontal deformation in the direction perpendicular to animal motion. Note that $\boldsymbol{\tau}(u,v,0)$

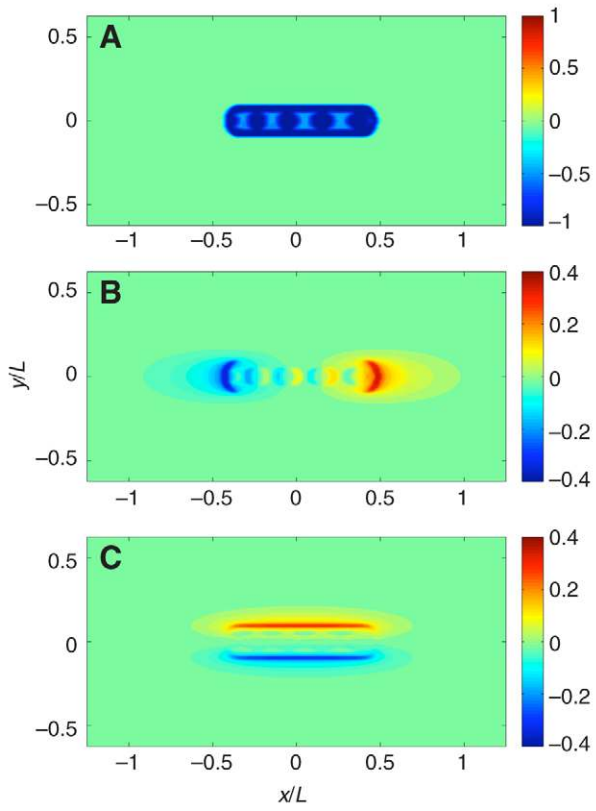

Fig. A1. Estimation of the error introduced in the traction force measurements by neglecting the weight of the animal. (A) Two-dimensional map of the synthetic weight distribution used in this estimation. The animal is moving from left to right. (B) Error in the horizontal shear stress distribution along the direction of motion of the animal for the synthetic weight distribution shown in A. Note that the upper and lower bounds of the color map have been decreased compared with panel A. (C) Error in the horizontal shear stress distribution normal to the direction of motion of the animal for the synthetic weight distribution in panel A. Note that the upper and lower bounds of the color map have been decreased compared with panel A. y/L and x/L, longitudinal and transverse distance to the animal's centroid, respectively, normalized by the length of the animal.

are the stresses obtained by our force measurement method, implying that $\boldsymbol{\tau}(0,0,W)$ is the error of the method. Therefore, we can estimate the error associated by neglecting the weight of the animal by calculating for a distribution of W that represents the normal stresses caused by the weight.

We have calculated the synthetic distribution of normal stresses (Fig. A1A). The weight distribution is set equal to –1 under the interwaves and the rim, –0.5 under the waves and zero on the surface of the substrate that is not in contact with the animal. The synthetic animal has four waves and is moving from left to right. This distribution was smoothed out with a box window of size $0.03L$ in order to avoid Gibbs error in the calculations. The errors in the horizontal shear stresses are shown in Fig. A1A,C. Note that the upper and lower limits of the color maps in these two figures have been decreased compared with Fig. A1A to yield a clear visualization. The order of magnitude of these errors is equal to the Poisson ratio, which is $\sigma \approx 0.3$ for the substrates used in this study. By comparing the error distributions in Fig. A1B with the propulsive force measurements in Fig. 16C,D, and the error distributions in Fig. A1C with the measurements in Fig. 16E,F, we can conclude that these errors do not modify the results for two reasons. First, the magnitude of the errors shown here are lower than the measured stresses by more than a factor of 2 and, for the stresses along the direction of motion, by up to a factor of 10. Second, the stress patterns observed in Fig. 16 differ qualitatively from the patterns in Fig. A1. In particular, the stresses in the direction perpendicular to motion pull inward towards the centerline of the animal whereas the error tractions push outward.

ACKNOWLEDGEMENTS

The authors would like to thank Dr Janet Leonard (UC Santa Cruz) for valuable discussions and for providing us with the banana slugs used in our experiments. Robbie Shepherd, Tran Nguyen and Kai Szeto assisted J.L. with some experiments. María Vázquez-Torres assisted in the measurements of the thickness of the foot–substrate gap. The work was supported by funds from the endowment of the Stanford and Beverly Penner Chair for Applied Sciences.

REFERENCES

Barr, R. A. (1926). Some observations on the pedal gland of *Milax*. *Q. J. Microsc. Sci.* **70**, 647-667.
Barr, R. A. (1927). Some notes on the mucous and skin glands of *Arion ater*. *Q. J. Microsc. Sci.* **71**, 503-525.
Brackenbury, J. (1999). Fast locomotion in caterpillars. *J. Insect Physiol.* **45**, 525-533.
Chan, B., Balmforth, N. J. and Hosoi, A. E. (2005). Building a better snail: lubrication and adhesive locomotion. *Phys. Fluids* **17**, 113101.
Chan, B., Ji, S., Kovea, C. and Hosoi, A. E. (2007). Mechanical devices for snail-like locomotion. *J. Intell. Mater. Syst. Struct,* **18**, 111-116.
Crozier, W. J. and Pilz, G. F. (1924). The locomotion of limax. I. Temperature coefficient of pedal activity. *J. Gen. Physiol.* **6**, 711-721.
del Alamo, J. C., Meili, R., Alonso-Latorre, B., Rodriguez-Rodriguez, J., Aliseda, A., Firtel, R. A. and Lasheras, J. C. (2007). Spatio-temporal analysis of eukaryotic cell motility by improved force cytometry. *Proc. Natl. Acad. Sci. USA* **104**, 13343-13348.
del Alamo, J. C., Rodríguez-Rodríguez, J., Lai, J. and Lasheras, J. C. (2008). The locomotion of marine and terrestrial gastropods: can the acceleration of the ventral pedal waves contribute to the generation of net propulsive forces? In *61st Annual Meeting of the APS Division of Fluid Dynamics*. San Antonio, TX.
Denny, M. W. (1980a). Locomotion – the cost of gastropod crawling. *Science* **208**, 1288-1290.
Denny, M. W. (1980b). The role of gastropod pedal mucus in locomotion. *Nature* **285**, 160-161.
Denny, M. W. (1981). A quantitative model for the adhesive locomotion of the terrestrial slug, *Ariolimax columbianus*. *J. Exp. Biol.* **91**, 195-217.
Denny, M. W. (1984). Mechanical-properties of pedal mucus and their consequences for gastropod structure and performance. *Am. Zool.* **24**, 23-36.
Denny, M. W. and Gosline, J. M. (1980). The physical-properties of the pedal mucus of the terrestrial slug, *Ariolimax columbianus*. *J. Exp. Biol.* **88**, 375-393.
Dubois, R. and Vles, F. (1907). Locomotion des Gasteropodes. *Compt. Rend. Acad. Sci. Paris* **144**, 658-659.
Full, R., Yamauchi, A. and Jindrich, D. (1995). Maximum single leg force production: cockroaches righting on photoelastic gelatin. *J. Exp. Biol.* **198**, 2441-2452.
Harris, A. K., Wild, P. and Stopak, D. (1980). Silicone rubber substrata: a new wrinkle in the study of cell locomotion. *Science* **208**, 177-179.
Harris, J. K. (1978). A photoelastic substrate technique for dynamic measurements of forces exerted by moving organisms. *J. Microsc.* **114**, 219-228.
Jones, H. D. (1973). Mechanism of locomotion of *Agriolimax reticulatus* (Mollusca: Gastropoda). *J. Zool.* **171**, 489-498.
Jones, H. D. (1975). *Locomotion*. New York: Academic Press.
Keer, L. M. (1964). Stress distribution at the edge of an equilibrium crack. *J. Mech. Phys. Solids* **12**, 149-163.
Kim, B., Lim, H. Y., Park, J. H. and Park, J. O. (2006). Inchworm-like colonoscopic robot with hollow body and steering device. *JSME Int. J. Ser. C* **49**, 205-212.
Lauga, E. and Hosoi, A. E. (2006). Tuning gastropod locomotion: modeling the influence of mucus rheology on the cost of crawling. *Phys. Fluids* **18**, 113102.
Lissmann, H. W. (1945a). The mechanism of locomotion in gastropod molluscs. 1. Kinematics. *J. Exp. Biol.* **21**, 58-69.
Lissmann, H. W. (1945b). The mechanism of locomotion in gastropod molluscs. 2. Kinetics. *J. Exp. Biol.* **22**, 37-50.
Meili, R., Alonso-Latorre, B., del Alamo, J. C., Firtel, R. A. and Lasheras, J. C. (2010). Myosin II is essential for the spatiotemporal organization of traction forces during cell motility. *Mol. Biol. Cell* **21**, 405-417.
Parker, G. H. (1911). The mechanism of locomotion in gastropods. *J. Morphol.* **21**, 155-170.
Quillin, K. J. (1999). Kinematic scaling of locomotion by hydrostatic animals: ontogeny of peristaltic crawling by the earthworm *Lumbricus terrestris*. *J. Exp. Biol.* **202**, 661-674.
Willert, C. E. and Gharib, M. (1991). Digital particle image velocimetry. *Exp. Fluids* **10**, 181-193.